Ceramics International 42 (2016) 8140–8150

Contents lists available at ScienceDirect

Ceramics International

journal homepage: www.elsevier.com/locate/ceramint

High emissivity $MoSi_2$–ZrO_2–borosilicate glass multiphase coating with SiB_6 addition for fibrous ZrO_2 ceramic

Gaofeng Shao [a,b], Xiaodong Wu [a,b], Sheng Cui [a,b,*], Xiaodong Shen [a,b,*], Yong Kong [a,b], Yucao Lu [a,b], Chunrong Jiao [c], Jian Jiao [c]

[a] State Key Laboratory of Materials-Oriented Chemical Engineering, College of Materials Science and Engineering, Nanjing Tech University, Nanjing 210009, China
[b] Nanjing Tech University Suqian Advanced Materials Institute, Suqian 223800, China
[c] National Key Laboratory of Advanced Composite, Beijing Institute of Aeronautical Materials, Beijing 101300, China

ARTICLE INFO

Article history:
Received 13 January 2016
Accepted 3 February 2016
Available online 9 February 2016

Keywords:
SiB_6
High emissivity coating
Fibrous ZrO_2 ceramic
Thermal shock behavior

ABSTRACT

To develop a high emissivity coating on the low thermal conductivity ZrO_2 ceramic insulation for reusable thermal protective system, the $MoSi_2$–ZrO_2–borosilicate glass multiphase coatings with SiB_6 addition were designed and prepared with slurry dipping and subsequent sintering method. The influence of SiB_6 content on the microstructure, radiative property and thermal shock behavior of the coatings has been investigated. The coating prepared with SiB_6 included the top dense glass layer, the surface porous coating layer and the interfacial transition layer, forming a gradient structure and exhibiting superior compatibility and adherence with the substrate. The emissivity of the coating with 3 wt% SiB_6 addition was up to 0.8 in the range of 0.3–2.5 μm and 0.85 in the range of 0.8–2.5 μm at room temperature, and the "V-shaped grooves" surface roughness morphology had a positive effect on the emissivity. The MZB-3S coating showed excellent thermal shock resistance with only 1.81% weight loss after 10 thermal cycles between 1773 K and room temperature, which was attributed to the synergistic effect of porous gradient structure, self-sealing property of oxidized SiB_6 and the match of thermal expansion coefficient between the coating and substrate. Thus, the high emissivity $MoSi_2$–ZrO_2–borosilicate glass coating with high temperature resistance presented a promising potential for application in thermal insulation materials.

1. Introduction

High friction heat resulting from the acute friction between a vehicle surface and the atmosphere leads to a severe increase in surface temperature during hypervelocity flights, which leads to reduced lifetime and performance of space vehicles material. The reusable thermal protective system (RTPS) consisting of high emissivity coatings used on the surface and a low conductivity insulation used inside could decrease the surface temperature by radiation and prevent heat transfer via thermal conduction. A mathematical model proposed by Van Wie [1] suggested that under an identical heat flux the wall temperature of a hypersonic vehicles is reduced by 573 K when its surface emissivity is increased from 0.5 to 1.0 at Mach 10. Alfano and Guazzoni et al. [2,3] also stated that radiation heat transfer is the only method for heating and cooling in outer space applications. Clearly, optimizing the emissivity can make a significant difference in reducing the surface temperature. Recently, porous fibrous ZrO_2 ceramics with "bird's nest" structure have been considered as a candidate material for thermal insulation under conditions of ultra-high temperatures and in various harsh environments due to the outstanding characteristics, including low density, extreme high-temperature stability and low thermal conductivity [4]. Thus, as a logical choice, a high emissivity coating must be designed and prepared on the fibrous ZrO_2 ceramic insulation substrate.

To date, a series of high emissivity coatings have been designed and prepared on the alloys and ceramic matrix composites for thermal protective system, including SiC [2,5,6], metal oxides(γ-Al_2O_3 [7], TiO_2 [8], SiO_2 [9], ZrO_2 [10]), rare-earth oxide(CeO_2 [11]), transition metal modified $LaMgAl_{11}O_{19}$ system [12,13], etc.. In addition to the pursuit of high emissivity, the other properties such as thermal shock resistance and oxidation resistance, should be also taken into account when high emissivity coatings are used at high temperatures [14]. However, single component coating

* Corresponding authors at: State Key Laboratory of Materials-Oriented Chemical Engineering, College of Materials Science and Engineering, Nanjing Tech University, Nanjing 210009, China. Tel.: +86 25 83587234; fax: +86 25 83221690.
E-mail addresses: shaogf@njtech.edu.cn (G. Shao), scui@njtech.edu.cn (S. Cui), xdshen@njtech.edu.cn (X. Shen).

http://dx.doi.org/10.1016/j.ceramint.2016.02.020
0272-8842/

could rarely possess these comprehensive properties. Designing multiphase coatings has been considered an effective way to solve the problem. The multiphase coating comprises of at least two phase: a crystalline phase and an amorphous phase, or two different crystalline phases, in which at least one is capable of absorbing and re-radiating thermal energy named as emissivity agent. The other phase is like a binder, which can provide high strength, thermal expansion characteristics similar to their intend substrates, and adequate bond strength with the substrate [15].

$MoSi_2$ is a potential matrix material for high temperature application, and it was widely researched in the fields of oxidation protective coating [16,17], high emissivity coating [18,19] and heating elements because of its high melting point (2293 K), prominent high-temperature oxidation resistance (1973 K) and corrosion resistance and high emissivity [20]. Among the binders, SiO_2 glass does not exhibit attractive viscosity and wetting characteristics as a binder. Although B_2O_3 glass combines thermal stability with appropriate viscosity and wetting to provide protection over a wide temperature range both as a coating and a sealant, this material volatilizes rapidly at high temperatures. The best compromise should be a thermally stable borosilicate glass with a high melting point and appropriate wetting properties and viscosity [21–23]. In our previous study, $MoSi_2$–borosilicate glass coating was developed for fibrous ZrO_2 ceramic insulation, though the emissivity of the coatings were reached 0.8, the thermal shock behavior was undesirable, and quite a few cracks are unavoidable in the coating during thermal shock tests [18]. ZrO_2 is an intensely attractive alternative reinforcing phase for $MoSi_2$, the addition of ZrO_2 into $MoSi_2$ may block the path of oxygen diffusion, therefore restrain the pest oxidation [24]. Besides, the addition of ZrO_2 could solve the mismatch of the coefficient of thermal expansion between fibrous ZrO_2 ceramics and the coating. Furthermore, ZrO_2 possesses high melting point, high emissivity at high temperature [25] and can react with SiO_2 to produce $ZrSiO_4$, which exhibits excellent chemical stability, high melting point and infrared emissivity [26]. The last but not the least, to improve the thermal stability of borosilicate glass, ZrO_2 was added into as introduced in some recent investigations [27]. Considering the advantages mentioned above, introducing ZrO_2 into $MoSi_2$–borosilicate glass coating would be a potential design to form the $MoSi_2$–ZrO_2–borosilicate glass coating on the fibrous ZrO_2 ceramic insulation. Moreover, SiB_6 exhibited excellent self-healing property due to the formation of borosilicate glass (including SiO_2 and B_2O_3) at high temperature [28], which not only can remain as a flux after being oxidized during the preparation process to fusion at the sintering temperature [29], but also can seal the micro-defects (holes or cracks) and improving the oxidation resistance and thermal shock resistance [16,30].

In the present work, a high emissivity $MoSi_2$–ZrO_2–borosilicate glass multiphase coating system was prepared on fibrous ZrO_2 ceramic insulation using $MoSi_2$ as high emittance agent, borosilicate glass as binder, ZrO_2 as a reinforced phase and SiB_6 as annexing agent by slurry dipping and subsequent sintering method. The effect of SiB_6 content on the microstructure, radiative property and thermal shock behavior of the as-prepared coatings were investigated.

2. Experimental

2.1. Preparation of the coatings

Fibrous ZrO_2 ceramics (25 mm × 25 mm × 5 mm and 15 mm × 15 mm × 5 mm) (Anhui Crystal New Materials Co. Ltd., China) with a density of 0.47 g/cm^3 were used as the substrates. The large size substrates (25 mm × 25 mm × 5 mm) were used for radiation property test, while the small size substrates (15 mm × 15 mm × 5 mm) were used for thermal shock test. A schematic diagram showing the oriented structure of the material is presented in Fig. 1(a), and the microstructure of the fibrous ZrO_2 ceramic in the plane of orientation of fibers (*XY* plane) is shown in Fig. 1(b). This plane is perpendicular to the direction of minimum thermal conductivity, and it can be observed that the fibrous ZrO_2 ceramic can build a "birds nest" structure to obtain high porosity, low thermal conductivity and relatively high strength.

A slurry was pre-prepared by method of ball milling. $MoSi_2$ (Beijing HWRK Chem Co.,Ltd, China), ZrO_2 (Sinopharm Chemical Reagent Co., Ltd, China), homemade high silica borosilicate glass which was reported in Ref. [18] and SiB_6 (Alfa Aesar, MA, USA), ethanol and silica sol were mixed in nylon ball-milling container and ball milled by a planetary mill for 12 h at a rotation speed of 300 rpm, where mass ratio of the powders, ethanol, silica sol and zirconia balls = 1:1:0.1:2, and the compositions of the coatings were listed in Table 1. Eventually, the particle size reached approximately 1–2 μm and the reduced particle size allowed effective impregnation of the outer surface. The coatings were prepared on the surface of the treated fibrous ZrO_2 ceramic using the dip-coating process. The coating thickness was controlled by the dipping times. After drying at 333 K for 4 h and at 373 K for 2 h, the

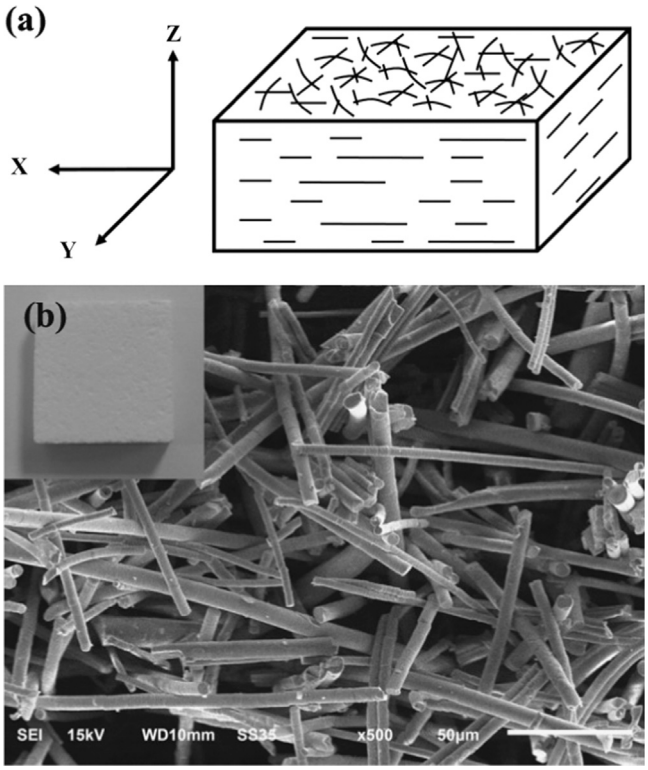

Fig. 1. (a) Schematic representation of fibrous ZrO_2 ceramic (b) SEM micrograph of fibrous ZrO_2 ceramic: *XY* plane (inset refers to the photograph of fibrous ZrO_2 ceramic).

Table 1
The compositions of the coatings.

Samples	Composition (wt%)			
	$MoSi_2$	ZrO_2	Borosilicate glass	SiB_6
MZB	40	10	50	–
MZB-1S	40	10	49	1
MZB-3S	40	10	47	3
MZB-5S	40	10	45	5

as-coated samples were then inserted into the furnace at 1573 K for 10 min in air and cooled by rapid removal from the furnace at atmospheric pressure to minimize stress in the coating.

2.2. Radiation property test

Reflectance spectra in the range of 0.3–2.5 μm were measured using a UV–vis–NIR spectrophotometer (UVPC measurement software, Shimadzu; Varian Cary5000, Varian), with $BaSO_4$ as the reflectance sample. The total emissivity can be derived from the reflectance spectrum according to Eq. (1):

$$\epsilon_T = \frac{\int_{\lambda_1}^{\lambda_2}[1 - R(\lambda)]P_B(\lambda)d\lambda}{\int_{\lambda_1}^{\lambda_2}P_B(\lambda)d\lambda} \quad (1)$$

where λ is the wavelength, $R(\lambda)$ is the reflectance, $P_B(\lambda)$ is given by Planck's law, which is calculated according to Eq. (2):

$$P_B(\lambda) = \frac{C_1}{\lambda^5[\exp(C_2/\lambda T) - 1]} \quad (2)$$

where $C_1 = 3.743 \times 10^{-16}$ Wm^2, C_2=1.4387 × 10^{-2} mK. Calculation of the total emissivity was performed using a MATLAB program that incorporated Eqs. (1) and (2).

2.3. Thermal shock behavior

To investigate the thermal shock resistance of the coating, thermal cycling tests of coated specimens were performed between 1773 K and room temperature in air. Specimens were put directly into the furnace of 1773 K for 10 min, and then were taken out of the furnace for 10 min. Then, the specimens were put directly into the furnace again for the next thermal cycle. At the designated time, the weight of these specimens was measured by the electronic balance with a sensitivity of ±0.1 mg. Weight change percentage ($\Delta W\%$) of the specimens was calculated by the following equation:

$$\Delta W\% = \frac{m_0 - m_1}{m_0} \times 100\% \quad (3)$$

where m_0 and m_1 are the weights of the specimens before oxidation and after oxidation, respectively.

2.4. Thermal expansion coefficient test

The linear thermal expansion behaviors of fibrous ZrO_2 ceramic, $MoSi_2$ and ZrO_2 using the bulk specimens have dimensions of approximately 5 mm × 5 mm × 20 mm were determined with a high-temperature dilatometer (Netzsch DIL 402C, Germany) from 323 K to 1673 K in Ar atmosphere. Data was continuously recorded at a heating rate of 10 K/min during heating, and they were corrected using the known thermal expansion of a certified standard alumina.

2.5. Characterization of the coatings

The surface morphology was examined by using a confocal laser scanning microscope (CLSM). The CLSM images were obtained on an Olympus LEXT OLS 4000 microscope powered by a singer laser (λ=405 nm) in the reflected light mode. The microstructure and the element distribution were surveyed using a scanning electron microscope (SEM, Model JSM-6510, JEOL, Tokyo, Japan) equipped with energy dispersive spectroscopy (EDS). The phase composition of the coating surface was examined using a Rigaku Miniflex X-ray diffractometer (XRD) with Cu-Kα radiation (λ=0.15406 nm).

3. Results and discussion

3.1. Microstructure of the coatings

XRD patterns of $MoSi_2$–ZrO_2–borosilicate glass coating surfaces with different SiB_6 content are presented in Fig. 2. SiB_6 tends to be oxidized above 873 K following Eq. (4) [28], making the SiB_6 phase undetected in XRD patterns. The amorphous nature of glass near 22° can be observed, indicating that the coating surfaces include the borosilicate glass, especially MZB-3S and MZB-5S coating surfaces, which is because the oxidation products (SiO_2 and B_2O_3) of SiB_6 with high contents could react to form amorphous borosilicate glass phase. The crystalline SiO_2 in MZB and MZB-1S coating surfaces is not only the oxidation of SiB_6 and $MoSi_2$ during the soaking at 1573 K according to Eqs. (4)–(7) but also from the partial borosilicate glass crystallized during the following cooling process. Consequently, with the increase of SiB_6 content, crystalline SiO_2 phase gradually decreases and eventually disappear, meanwhile the amorphous phase gradually increases and covers the coating surfaces. Moreover, no visible $MoSi_2$ peaks are found in MZB-3S and MZB-5S coating surfaces, therefore we can deduce that the glass layer is thick enough to protect the X-ray from penetrating it, since XRD penetration is typically within ten-odd to tens micrometers related to the tested materials. Additionally, Mo_5Si_3, MoO_2 and Mo are supposed to form from the productions of the slight oxidation of $MoSi_2$ according to Eqs. (5)–(7). As shown in Fig. 3, the Gibbs-free energy, ΔG, for reactions (4)–(7) at different temperatures ranging from 473 K to 1873 K is calculated by the FACT program[31]. Negative ΔG suggests that these reactions are thermodynamically favorable and can occur under the heat-treatment process.

$$SiB_6(s) + 11/2O_2(g) = SiO_2(\text{most stable}) + 3B_2O_3(\text{most stable}) \quad (4)$$

$$MoSi_2(s) + 3O_2(g) = MoO_2(s) + 2SiO_2(s) \quad (5)$$

$$MoSi_2(s) + 2O_2(g) = Mo(s) + 2SiO_2(s) \quad (6)$$

$$MoSi_2(s) + 7/5O_2(g) = 1/5Mo_5Si_3(s) + 7/5SiO_2(s) \quad (7)$$

Fig. 4 shows the SEM images of the as-prepared $MoSi_2$–ZrO_2–borosilicate glass coating surfaces. It is clearly that MZB coating is dense but a visible crack appears (Fig. 4(a) and (e)). It may due to the mismatch of thermal expansion coefficient between the

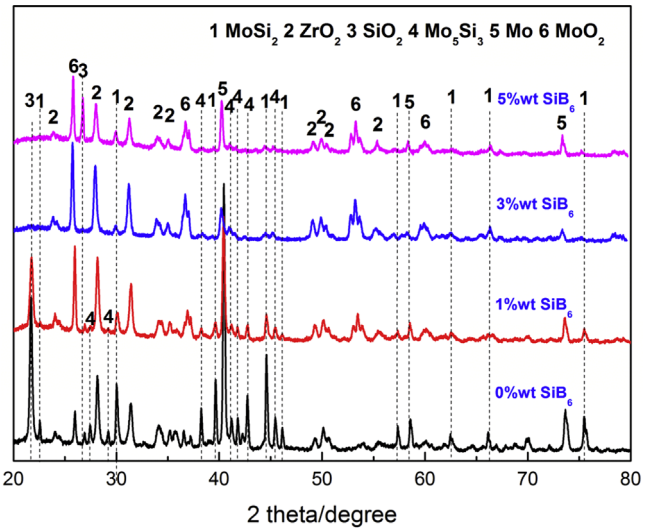

Fig. 2. XRD patterns of $MoSi_2$–ZrO_2–borosilicate glass coating surfaces with different SiB_6 contents.

coating and the substrate. Moreover, the existence of the α-cristobalite phase proves that silica-based glassy phase crystallized into β-cristobalite at 1573 K, and then the β-cristobalite undergoes a β→α displacive phase transition when the temperature decreases to room temperature. This transition is often accompanied by 3–5% volume change and might generate thermal stresses, resulting in some micro-cracks of the coating [32]. After introducing SiB_6, it remains in the coating as a flux and oxidizes during processing to ensure fusion at the sintering temperature. The borosilicate glass formed from SiB_6 at high temperature can seal the defects, resulting in no obvious micro-cracks in the coatings (Fig. 4 (f)–(h)). Nonetheless, more or less pores are observed on the surface of the MZB-1S, MZB-3S, MZB-5S coatings except the MZB coating, as blue arrows indicated in Fig.4(b)–(d), the number of the pores in the coatings decreases and the size of the pores in the coatings decreases firstly and then increases with increasing content of SiB_6. The MZB-1S coating with less SiB_6 cannot form a thick glass layer, which results in some pores formed by emission of gaseous byproducts (Fig. 4(b)). With the increase of SiB_6, an borosilicate glass with appropriate wetting and viscosity is generated in MZB-3S coating, which can seal the pores as well as decrease the size and the amount of holes (Fig. 4(c)). However, B_2O_3-rich borosilicate glass is presumably generated in the MZB-S5 coating surface with the highest content of SiB_6 addition, and once the temperature exceeds 1473 K, the evaporation of B_2O_3 begins to occur, leading to some big pores in the surface (Fig. 4(d)).

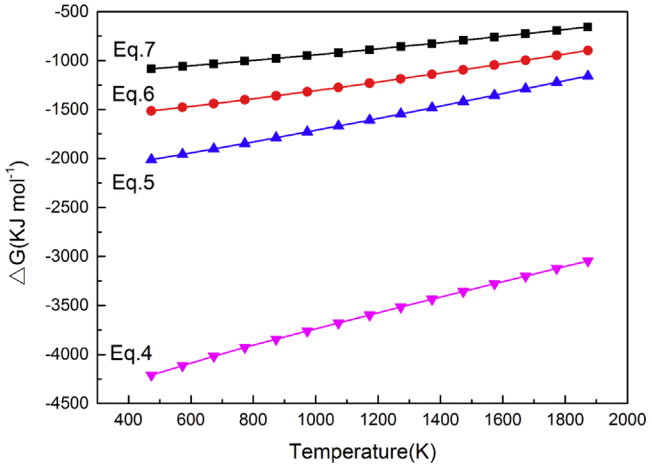

Fig. 3. Gibbs-free energy for reaction (1)–(4).

By EDS and XRD analyses, the surface glass layer of MZB-1S, MZB-3S, MZB-5S coatings can be identified as Zr–Si–O glass containing "pinning phase ZrO_2". No obvious EDS peaks of B are observed because it is a light element.

Cross-section SEM images of the $MoSi_2$–ZrO_2–borosilicate glass coating with 3 wt% SiB_6 addition are shown in Fig. 5. Obviously, it could be divided into three layers of MZB-3S coatings (Fig. 5(a)): the top glass layer (I), the dense surface coating layer (II) and the interfacial transition layer (III). The top glass layer is dense and the density of the top glass layer mainly depends on the oxide from ceramic oxide reacts and molten borosilicate glass. Below this layer is the surface coating layer, from which it can be seen that the coating is porous and with the thickness about 200 μm, and the density of this layer is mainly depends on molten borosilicate glass. Thus, it appears that the top glass layer is more compact than the surface coating layer. Moreover, the interface between layer (I) and layer (II) appears to be continuous, and no interfacial gaps are detected. In the interfacial transition layer (III), part of the coating material has infiltrated into the substrate through the open pores of fibrous ZrO_2 ceramic insulation. Therefore, the obtained coating has a pleasurable combination with the substrate, and no obvious delamination is discovered, which is beneficial to increasing the compatibility and adherence between the coatings and the substrate. Consequently, the gradient distributions of the porous structures along the thickness direction of coating were designed. For the top dense coating, it can be used for waterproof and antioxidant, and the porous coating can be used for enhancing the adhesion and thermal shock resistant. The gradient coating combines the advantages of the top dense coating and the surface porous coating and is very suitable for porous fibrous ceramic [19].

To observe the difference of the cross-section morphology of the coatings with different SiB_6 content, the cross-section CLSM images and BSE images of the $MoSi_2$–ZrO_2–borosilicate glass coatings are shown in Fig. 6. It can be identified that the thickness of MZB, MZB-1S, MZB-3S, MZB-5S surface coating layers are approximately 160 μm, 190 μm, 190 μm, 220 μm, respectively. Obviously, it could be divided into three layers of coatings: the top oxidation layer, the dense surface coating layer and the interfacial transition layer. On the top of the coatings are oxidation layers which can be recognized manifestly in BSE images (Fig. 6(e)–(h)). The thickness of the oxidation layer of MZB, MZB-1S, MZB-3S, MZB-5S are approximately 3 μm, 10 μm, 30 μm, 70 μm, respectively, which increases with SiB_6 addition. Whist, some bubbles and pores are observed in the oxidation layer, especially MZB-3S and MZB-5S coatings, which is caused by the evaporation of B_2O_3.

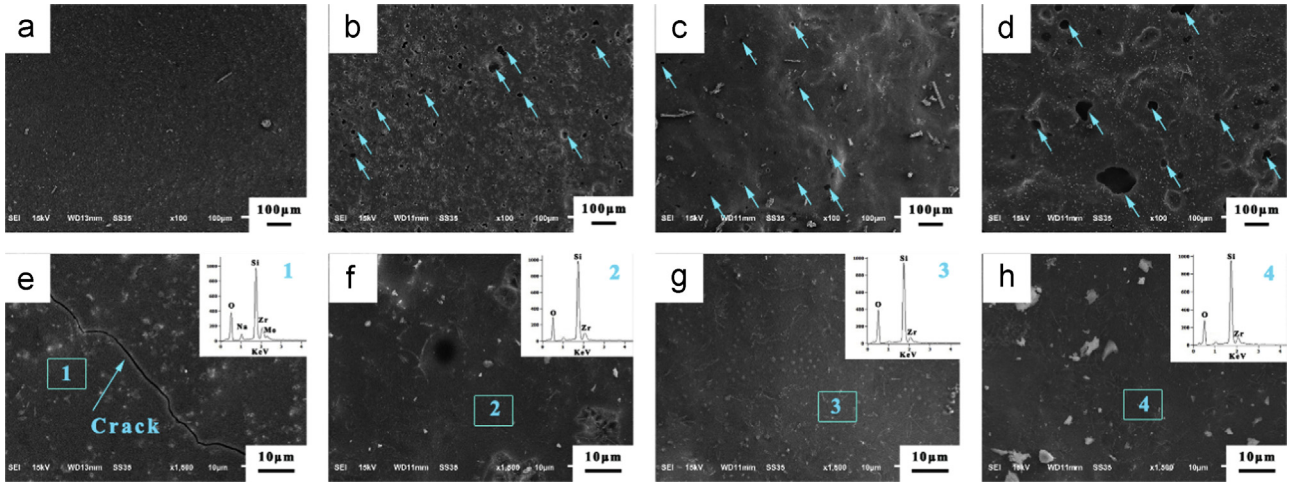

Fig. 4. Surface SEM images of the $MoSi_2$–ZrO_2–borosilicate glass coating, (a, e) MZB; (b, f) MZB-1S; (c, g) MZB-3S; (d, h) MZB-5S. (For interpretation of the references to color in this figure, the reader is referred to the web version of this article.)

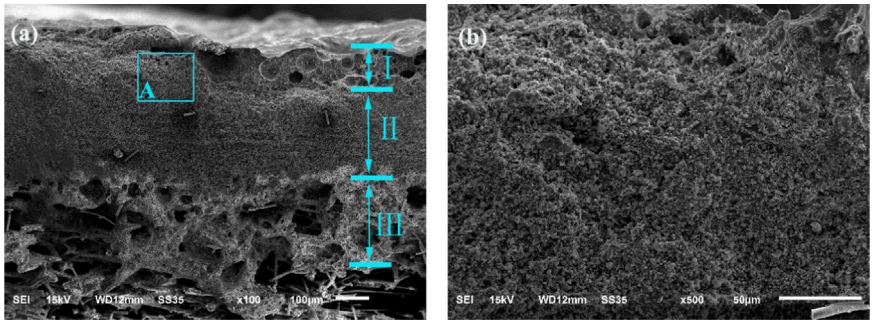

Fig. 5. (a) Cross-section SEM image of the $MoSi_2$–ZrO_2–borosilicate glass coating with 3 wt% SiB_6 addition; (b) magnification of part A in (a).

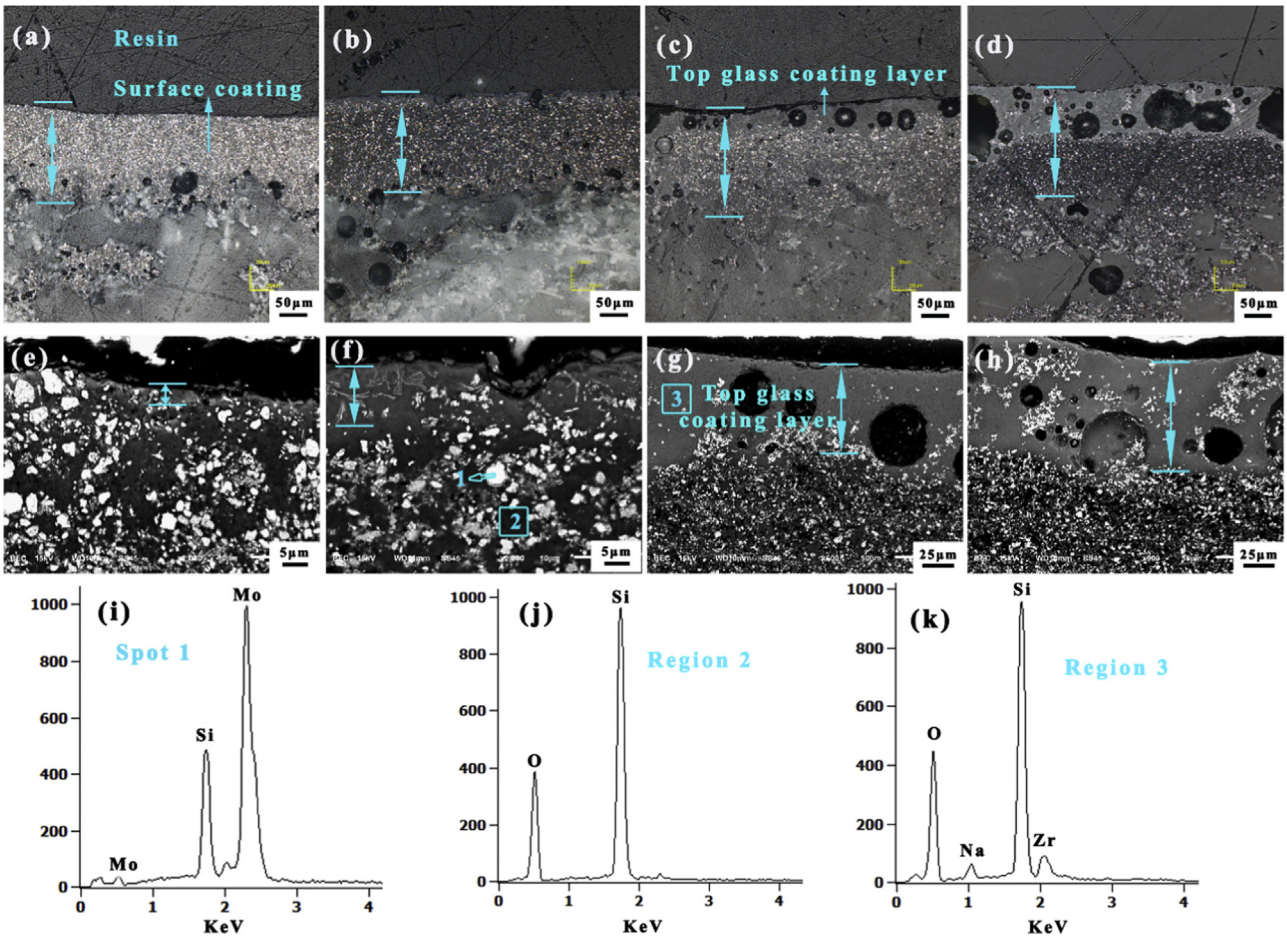

Fig. 6. CLSM (a–d) and BSE (e–h) images of the $MoSi_2$–ZrO_2–borosilicate glass coatings, (a, e) MZB; (b, f) MZB-1S; (c, g) MZB-3S; (d, h) MZB-5S; (i–k) EDS analyses of the coatings.

By EDS analyses, the white, grey and black phases can be recognized as $MoSi_2$, Zr–Si–O composite glass, SiO_2 or borosilicate glass, respectively, which is consistent with the result of XRD.

The different structures observed above are achieved by adding different amount of SiB_6 which can control the formation of liquid phase during sintering. After introducing SiB_6, there will be two kinds of borosilicate glass existing in the coating, one is SiO_2-riched borosilicate glass which comes from the original powders, the other is B_2O_3-riched borosilicate glass which generated from the oxidation of SiB_6 during sintering. Eventually, both of the borosilicate glasses will fuse together to form a new borosilicate glass, an increase in the SiB_6 content will promote the generation of B_2O_3-riched borosilicate glass and decrease the viscosity of the new borosilicate glass under high temperature due to the decrease of the melting point of borosilicate liquid phase. Some studies have indicated that in the SiO_2-B_2O_3 system, when the content of B_2O_3 increased from 0.5 wt% to 5 wt%, the melting point of the borosilicate glass was reduced from 1700 °C to 1460 °C and the viscosity of borosilicate glass was decreased with the increase of B_2O_3, which is due to that the increased B_2O_3 enhanced the formation of non-bridged oxygen atoms in [BO_3]-triangular structural units transforming the 3-D complex network structures such as pentaborate and tetraborate to 2-D structures of boroxol and boroxyl rings. These changes to more simple structures lowered the viscosity [33]. Therefore a slight change in the amount of SiB_6 can significantly change the structure of the prepared coatings.

3.2. The radiation property of the coating

Fig. 7 shows the spectral emissivity/absorptivity curves of the

$MoSi_2$–ZrO_2–borosilicate glass coatings prepared with different SiB_6 content. There is no significant differences among the emissivity values of the coatings. The MZB-3S coating shows the highest emissivity than that of the other three in the wavelength of 0.3–2.5 μm, and the spectral emissivity of the MZB-5S coating is lower than the others, especially in the wavelength of 1.5–2.5 μm. The calculated total emissivity values in various regions of wavelength are summarized in Table 2. In the range of 0.3–2.5 μm, the trend of the total emissivity is increasing first and then decreasing with the increase content of SiB_6, and the maximum value can rise to 0.8. Moreover, all kinds of the coatings are higher than 0.8 in the near-infrared range (0.8–2.5 μm), and the MZB and MZB-3S coatings can reach to 0.85. According to Wien's displacement law, $\lambda_{max}=b/T$, $b=2.8977721(26)\times10^{-3}$ m K; the blackbody intensity is maximum at a given temperature at wavelength λ_{max}, and this maximum shifts toward shorter wavelengths as the temperature is increased. Therefore, the higher the temperature, the more meaningful the emissivity of the short wavelength. The peak radiant intensity of a blackbody occurs at 1.73 μm at 1673 K and at 1.27 μm at 2273 K, in the range of 1.27–1.73 μm, the $MoSi_2$–ZrO_2–borosilicate glass coatings exhibit a high emissivity greater than 0.8, especially MZB and MZB-3S coatings, whose emissivity values reach to 0.85.

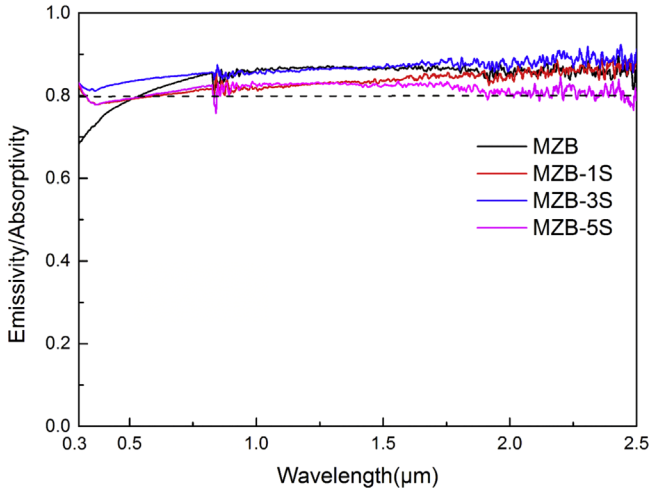

Fig. 7. Emissivity/absorptivity of the $MoSi_2$–ZrO_2–borosilicate glass coatings prepared with different SiB_6 contents.

As well known, not only the surface chemical composition, but also the surface morphology has a great influence on the emissivity of the coatings. A multitude of researchers have manifested that there is a positive link between the emissivity and the surface roughness [11,34,35]. Fig. 8 shows the surface roughness morphology and 3D surface roughness morphology gradient map of the MZB-3S coating. Whilst, the line profiles and roughness values of five different locations marked in Fig. 8(b) are presented in Fig. 8(c) and summarized in Table 3, respectively, which are obtained from a CLSM

Table 2
The calculated total emissivity values in various ranges of wavelength.

Sample	Calculated total emissivity		
	0.3–2.5 μm	0.8–2.5 μm	1.27–1.73 μm
MZB	0.7365	0.8550	0.8672
MZB-1S	0.7945	0.8226	0.8354
MZB-3S	0.8233	0.8576	0.8686
MZB-5S	0.7965	0.8208	0.8271

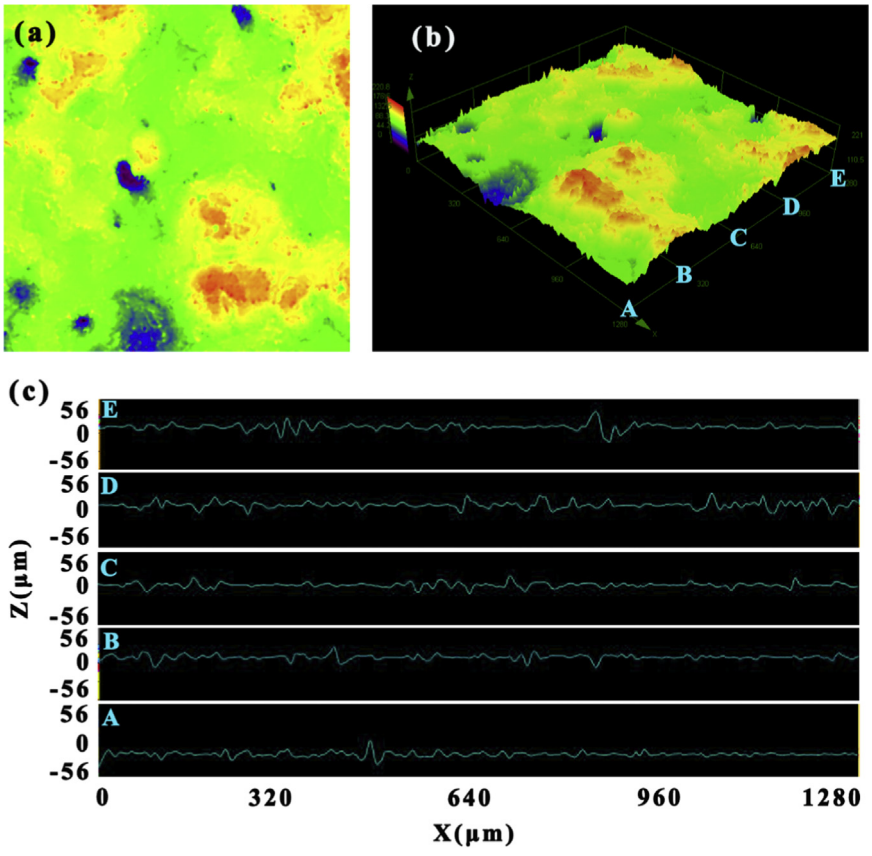

Fig. 8. (a) The surface roughness morphology of the coating (b) 3D surface roughness morphology gradient map of the coating (c) The roughness profiles of different positions marked in (b).

Table 3
The roughness values of five different locations.

Location	R_q (μm)	*Rsk* (μm)	σ/λ (λ=0.3–2.5 μm)
A	6.019	−0.033	>1
B	5.514	−0.249	>1
C	6.134	−0.030	>1
D	8.556	0.032	>1
E	6.924	0.091	>1

study. The root mean square roughness (R_q) calculates the root mean square average of the profile deviation from the mean line (i.e., the standard deviation of the height distribution): $R_q = \sqrt{\frac{1}{n}\sum_{i=1}^{n} Z_i^2}$. The skewness of the profile (*Rsk*) is the quotient of the mean cube value of the ordinate values $z(x)$ and the cube of Sq within the evaluation length: $Rsk = \frac{1}{R_q^3}\left(\frac{1}{n}, \sum_{i=1}^{n}, z_i^3\right)$, which provides a description of the asymmetry of the profile and it is close to zero for a Gaussian height distribution, whereas a positive values is indicative of a flat surface with peaks, and a negative value a bearing surface with valleys [36]. Wen et al. [37] divided the rough surfaces into three spectral regions based on optical roughness, which is represented by the ratio of root-mean-square (R_q) surface roughness, σ, to wavelength, λ namely: (1) Specular Region ($0 < \sigma/\lambda < 0.2$); (2) Intermediate Region ($0.2 < \sigma/\lambda < 1$); and (3) Geometric Region ($\sigma/\lambda > 1$). For the different locations marked with A,B,C,D,E of MZB-3S coating surface, the σ/λ ratio is greater than 1 in the region of ultraviolet to near infrared (λ=0.3–2.5 μm). Hence, the σ/λ ratio of the coating lies in the Geometric Region. In the Geometric Region, surfaces with a repeatable grooved finish, such as V-shaped grooves, circular grooves, and pyramidal grooves are commonly used to model the emissivity enhancement. Combining the roughness profiles shown in Fig. 8(c), "V-shaped grooves" model is more suitable to explain the phenomena of the enhanced emissivity for the coating. As we know, most of the electromagnetic wave was reflected, and only a little was absorbed by the coatings with a smooth surface. However, a significant absorptivity increase and reflectivity decrease by small gradual slopes in "V-shaped grooves" can be observed from the rough coating because multiple reflection will be caused by the slope of the "V-shaped grooves" surface. Therefore, compared with the smooth surface, the rough coatings exhibit lower reflectivity and higher absorptivity, which leads to high emissivity according to Kirchhoff's law of thermal radiation.

3.3. Thermal shock behavior of the coating

The weight change curves of $MoSi_2$–ZrO_2–borosilicate glass coated samples during the thermal shock test between 1773 K and room temperature are presented in Fig. 9. It can be seen that the weight of MZB coating decreases with the increase of thermal shock cycle, and weight loss of the coated sample is 7.36% after 10 cycles, which shows the poor oxidation protective ability and thermal shock resistance. However, the initial weight gains are observed in MZB-1S, MZB-3S and MZB-5S coatings, with a maximum of 1.29%, 3.57% and 1.19% after the first thermal shock cycle, then a continuous weight loss occurs, and the cumulated weight loss of MZB-3S coated sample is 1.81% after 10 cycles, which reveals the best thermal shock resistance.

To recognize the components on the surface of the coated samples, the XRD patterns of the coated samples after thermal shock test between 1773 K and room temperature are shown in Fig. 10. As shown in Fig. 10(a), it can be seen that $MoSi_2$, ZrO_2, SiO_2 and $ZrSiO_4$ are the main components on the surface of the MZB coating after 10 cycles, compared with the original components on the surface of the coating (Fig. 2(a)), Mo,MoO_2 and Mo_5Si_3 phases

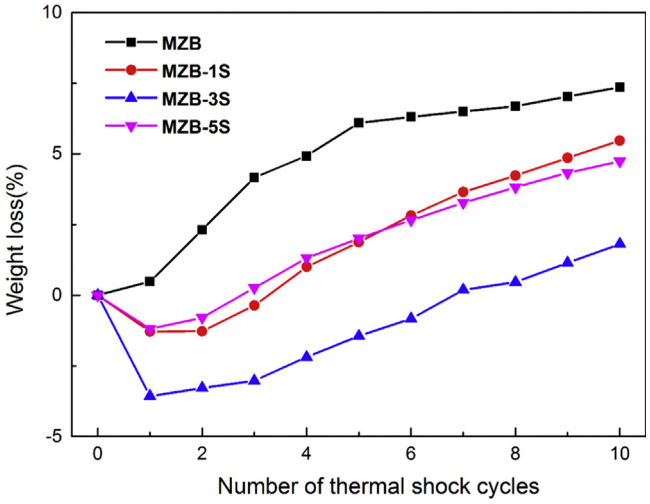

Fig. 9. Weight loss curves of $MoSi_2$–ZrO_2–borosilicate glass coated samples with different SiB_6 content during the thermal shock test.

have begun to oxidize to form the volatilizable products (MoO_3) according to Eqs. (5)–(8), which leads to the weight loss of the coated samples. Whist the $ZrSiO_4$ phase is generated on the surface of the coating, which is formed by ZrO_2 and SiO_2 according to Eq. (9) at high temperature. For the MZB-1S coated sample, as shown in Fig. 10(b), Mo, MoO_2 and Mo_5Si_3 phases still exist on the surface, which is because the thicker glass layer formed on the as-prepared MZB-S coating than MZB coating, retarding the oxidation and resulting in less weight loss. While for MZB-3S and MZB-5S coated samples, as shown in Fig. 10(c) and (d), three kinds of oxides can be detected, including $ZrSiO_4$, ZrO_2 and SiO_2. Combined with the board bump at 22° in XRD patterns, it can be concluded that the formation of Zr–Si–O compound layer with $ZrSiO_4$ dispersants generated on the surface of the coatings, which can decrease the diffusion rate of oxygen and improve stability of glassy layer [38].

$$MoSi_2(s)+3O_2(g)=MoO_3(g)+2SiO_2(s) \quad (8)$$

$$Mo_5Si_3(s)+21/2O_2(g)=5MoO_3(g)+3SiO_2(s) \quad (9)$$

$$Mo(s)+3/2O_2(g)=MoO_3(g) \quad (10)$$

$$ZrO_2(s)+SiO_2(s)=ZrSiO_4(s) \quad (11)$$

Fig. 11 shows the 3D surface morphology with CLSM images before and after 10 thermal shock cycling times. By observing the CLSM images (Fig. 11(a)–(d)), all of the as-prepared coating surfaces are glossy and crack free. The gloss is more and more bright with the increase of SiB_6 content which is ascribed to the more glass phase generated in the coatings. Whist, the distributions of pores on the surface of different coatings such as the size and the numbers are consisted with the SEM images shown in Fig. 4. After 10 cycling times, a porous layer is generated on the surface of the MZB coating (Fig. 11(e)), which is because that the evaporation of oxidation production (MoO_3) during thermal shock test. Moreover, the porous layer is mainly comprised of crystalline SiO_2, $ZrO_2$and $ZrSiO_4$ according to the result of XRD, compared with the amorphous glass phase, it can't seal the pores in the coating, resulting in the continuous weight loss of the MZB coated sample. As observed in Fig. 11(f), though a glass layer is form on the surface of the coating due to the addition of SiB_6, the glass phase is not sufficient to seal the pores. With the increase of SiB_6, a compound Zr–Si–O glass layer with appropriate wetting property and viscosity is generated on the surface of the MZB-3S coating, which leads to no micro-cracks and pores (Fig. 11(g)). Compared with the top glass

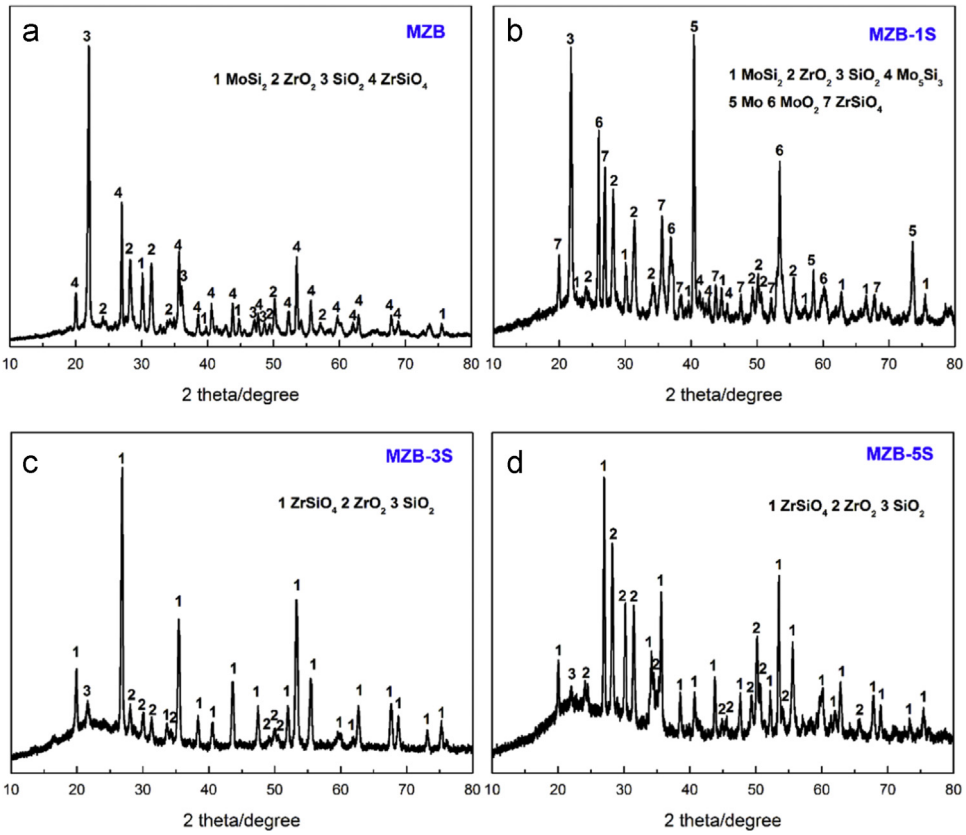

Fig. 10. XRD patterns of $MoSi_2$–ZrO_2–borosilicate glass coating surfaces with different SiB_6 content after 10 thermal shock cycles (a): MZB; (b): MZB-1S; (c): MZB-3S; (d): MZB-5S.

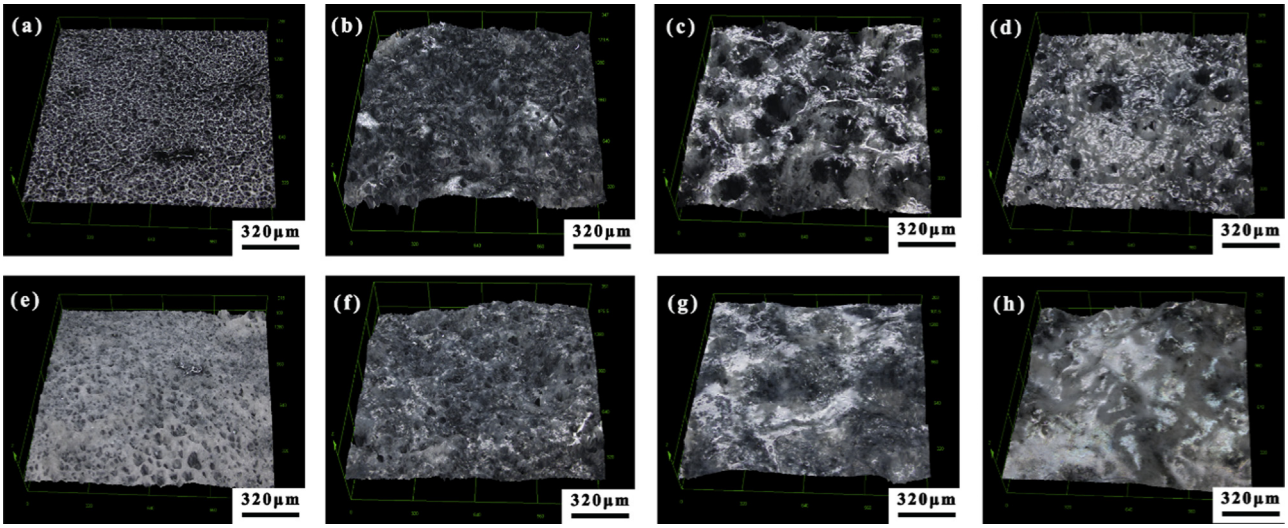

Fig. 11. 3D surface CLSM images of the $MoSi_2$–ZrO_2–borosilicate glass coatings before (a–d) and after (e–h) thermal shock test, (a, e) MZB; (b, f) MZB-1 S; (c, g) MZB-3 S; (d, h) MZB-5S;

layer of the MZB-3S coating, a thicker glass layer covers the MZB-5S coating (Fig. 11(h)).

Fig. 12 shows the surface SEM image of MZB-3S coating after 10 thermal shock cycles. It can be seen that a compound glass layer with some "immiscible phases" cover on the surface of MZB-3S coating, which forms a kind of "inlaid structure" (Fig. 12(a) and (b) shows the magnification of part A in Fig. 12(a). Combined with EDS (Fig. 12(c) and (d)) and XRD (Fig. 10(c)) analyses, region 1 and region 2 could be distinguished as $ZrSiO_4$ and amorphous SiO_2. The existence of $ZrSiO_4$ can highly improve the stability of silicate glass, which plays the role of "pinning effect"[39]. Furthermore, there is no micro-cracks generated on the surface of the coating, which demonstrated the excellent thermal shock resistance. Fig. 13 shows the cross-section SEM image of MZB-3S coated fibrous ZrO_2 ceramic. It could be divided into two layers of MZB-3S coating: the surface coating layer (I) and the interfacial transition layer (II). Some holes are formed in the surface coating layer, which is due to the volatilization of B_2O_3 and MoO_3 during the thermal shock test. However, the formed bubbled holes on the surface can hardly penetrate through the inner coating, they can be sealed with the

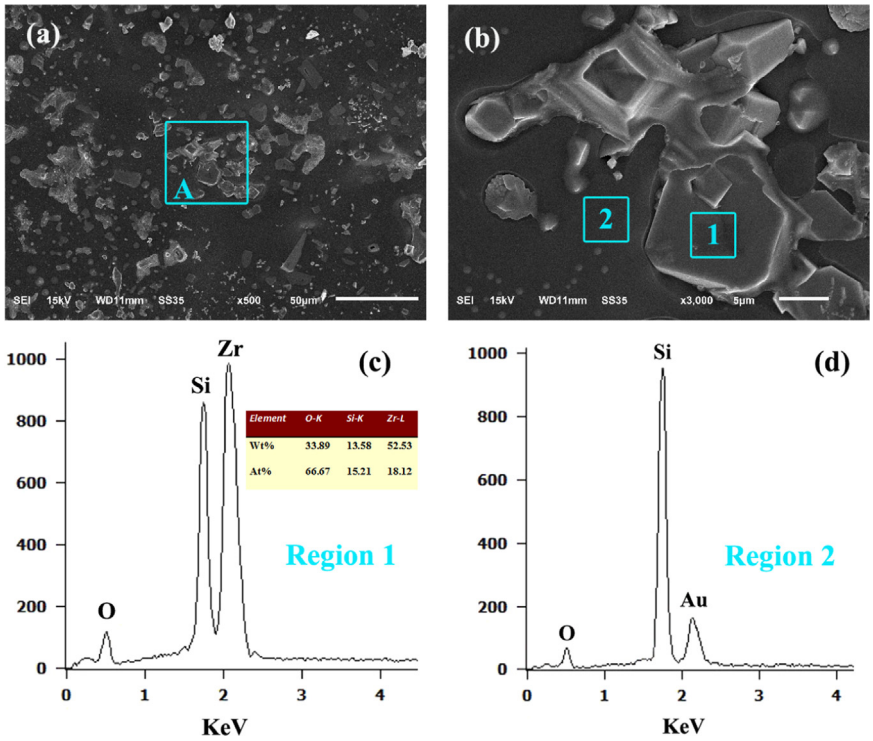

Fig. 12. (a) Surface SEM image of MZB-3S coating after 10 thermal shock cycles; (b) magnification of part A in (a); (c) and (d) regions EDS analyses in (b).

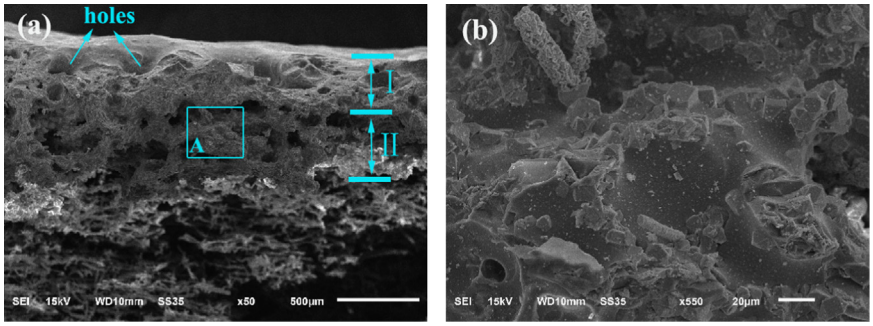

Fig. 13. (a) Cross-section SEM image of the $MoSi_2$–ZrO_2–borosilicate glass coating with 3 wt% SiB_6 addition after 10 thermal shock cycles; (b) magnification of part A in (a).

compound glass, which is helpful to prevent the coating from oxidation. Fig. 13(b) shows the magnification of part A in the interfacial layer in Fig. 13(a), a stable and densified glass phase is form to connect the surface coating layer and the substrate, and no obvious peeling off occurs on the interface. Thus, the dense surface coating layer can act as the functions of high emissivity and oxidation resistance, and the porous interfacial transition layer can reduce the thermal stress and improve the thermal shock resistance.

It was reported that the coating stress σ_c may be divided into three components: $\sigma_c = \sigma_t + \sigma_g + \sigma_a$, where σ_t is the CTE mismatch stress, σ_g is the growth stress and σ_a is the aging stress [40]. The growth stress is a stress that develops during the coating deposition. The aging stress is a stress that results from many aspects such as phase transformation, sintering, oxidation and chemical reactions of the coating [41]. In this work, the coating stress may consist mainly of the CTE mismatch stress and the aging stress. Fig. 14 shows the variations in thermal expansion rate with the temperature for $MoSi_2$, ZrO_2 and fibrous ZrO_2 ceramic, the average CTEs are 9.32×10^{-6}/K, 11.1×10^{-6}/K and 10.2×10^{-6}/K, which

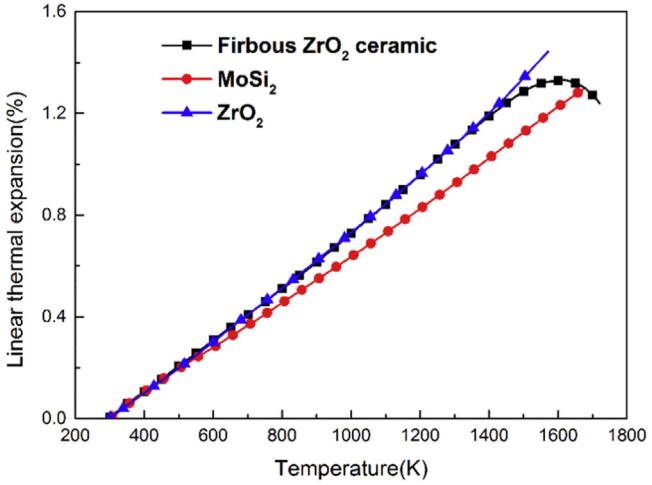

Fig. 14. Variations in thermal expansion rate with the temperature for $MoSi_2$, ZrO_2 and fibrous ZrO_2 ceramic.

shows a little mismatch between the coating and the substrate in consideration of the borosilicate glass composition in the coating, causing the CTE mismatch stress. The aging stress is formed due to the oxidation on the surface of the coating as well as the chemical reactions between ZrO_2 and SiO_2. Once the coating stress accumulated enough, the micro-cracks will be inevitable generated. However, no visible micro-cracks are detected during the thermal shock test, which can be briefly inferred as follows: (1) the similar thermal expansion coefficient between the coating and the substrate; (2) the porous structure can reduce the thermal stress; (3) the oxidized SiB_6 and borosilicate glass has a remarkable self-healing and crack-sealing functions.

4. Conclusions

A high emissivity $MoSi_2$–ZrO_2–borosilicate glass multiphase coating with SiB_6 addition on the low thermal conductivity ZrO_2 ceramic insulation has been successfully prepared with slurry dipping and subsequent sintering method. The coating prepared in the presence of 3 wt% SiB_6 included the top dense glass layer, the surface porous coating layer and the interfacial transition layer, forming a gradient structure and exhibiting good compatibility and adherence. The emissivity of the coating is up to 0.8 in the range of 0.3–2.5 μm and 0.85 in the range of 0.8–2.5 μm at room temperature, and the "V-shaped grooves" surface roughness morphology had a positive effect on the emissivity. The MZB-3S coating showed excellent thermal shock resistance with only 1.81% weight loss after 10 thermal cycles between 1773 K and room temperature, which was attributed to the synergistic effect of porous gradient structure, self-sealing property of SiB_6 and the match of thermal expansion coefficient between the coating and substrate. Thus the $MoSi_2$–ZrO_2–borosilicate glass coating is attractive for short-term applications for fibrous ZrO_2 ceramic insulation exposed to the temperature up to 1773 K.

Acknowledgments

This work was financially supported by the Program for Changjiang Scholars and Innovative Research Team in University (No. IRT_15R35), the Industry Program of Science and Technology Support Project of Jiangsu Province (No. BE2014128), the National Aerospace Science Foundation of China (No. 201452T4001), the Major Program of Natural Science Fund in Colleges and Universities of Jiangsu Province (No. 15KJA430005), the Prospective Joint Research Program of Jiangsu Province (No. BY2015005-01), Jiangsu Collaborative Innovation Center for Advanced Inorganic Function Composites and the Priority Academic Program Development of Jiangsu Higher Education Institutions (PAPD). Any opinions, findings, and conclusions or recommendations expressed in this paper are those of the authors and do not necessarily reflect the views of these programs.

References

[1] D.M. Van Wie, D.G. Drewry, D.E. King, C.M. Hudson, The hypersonic environment: required operating conditions and design challenges, J. Mater. Sci. 39 (2004) 5915–5924.
[2] D. Alfano, L. Scatteia, S. Cantoni, M. Balat-Pichelin, Emissivity and catalycity measurements on SiC-coated carbon fibre reinforced silicon carbide composite, J. Eur. Ceram. Soc. 29 (2009) 2045–2051.
[3] G.E. Guazzoni, High-temperature spectral emittance of oxides of Erbium, Samarium, Neodymium and Ytterbium, Appl. Spectrosc. 26 (1972) 60–65.
[4] J. Sun, Z. Hu, J. Li, H. Zhang, C. Sun, Thermal and mechanical properties of fibrous zirconia ceramics with ultra-high porosity, Ceram. Int. 40 (2014) 11787–11793.
[5] J. Yi, X. He, Y. Sun, Y. Li, Electron beam-physical vapor deposition of SiC/SiO_2 high emissivity thin film, Appl. Surf. Sci. 253 (2007) 4361–4366.
[6] F. Wang, L. Cheng, L. Xiang, Q. Zhang, L. Zhang, Effect of SiC coating and heat treatment on the thermal radiation properties of C/SiC composites, J. Eur. Ceram. Soc. 34 (2014) 1667–1672.
[7] Y.M. Wang, H. Tian, X.E. Shen, L. Wen, J.H. Ouyang, Y. Zhou, D.C. Jia, L.X. Guo, An elevated temperature infrared emissivity ceramic coating formed on 2024 aluminium alloy by microarc oxidation, Ceram. Int. 39 (2013) 2869–2875.
[8] Z.W. Wang, Y.M. Wang, Y. Liu, J.L. Xu, L.X. Guo, Y. Zhou, J.H. Ouyang, J.M. Dai, Microstructure and infrared emissivity property of coating containing TiO_2 formed on titanium alloy by microarc oxidation, Curr. Appl. Phys. 11 (2011) 1405–1409.
[9] X. Zhao, X.D. He, Y. Sun, L.D. Wang, Carbon nanotubes doped SiO_2/SiO_2–PbO double layer high emissivity coating, Mater. Lett. 65 (2011) 2592–2594.
[10] Z. Yao, Q. Xia, Q. Shen, P. Ju, P. Su, B. Hu, Z. Jiang, A facile preparation of ceramic coatings on Ti alloys for thermal protection systems, Sol. Energy Mater. Sol. Cells 143 (2015) 236–241.
[11] J. Huang, Y. Li, X. He, G. Song, C. Fan, Y. Sun, W. Fei, S. Du, Enhanced spectral emissivity of CeO_2 coating with cauliflower-like microstructure, Appl. Surf. Sci. 259 (2012) 301–305.
[12] H.Z. Liu, Z.G. Liu, J.H. Ouyang, Y.M. Wang, Influences of lattice vibration and electron transition on thermal emissivity of Nd^{3+} doped $LaMgAl_{11}O_{19}$ hexaaluminates for metallic thermal protection system, Appl. Phys. Lett. 101 (2012) 161903.
[13] H.Z. Liu, J.H. Ouyang, Z.G. Liu, Y.M. Wang, Thermo-optical properties of $LaMAl_{11}O_{19}$ (M=Mg, Mn, Fe) hexaaluminates for high-temperature thermal protection applications, J. Am. Ceram. Soc. 94 (2011) 3195–3197.
[14] H.Z. Liu, J.H. Ouyang, Z.G. Liu, Y.M. Wang, Microstructure, thermal shock resistance and thermal emissivity of plasma sprayed $LaMAl_{11}O_{19}$ (M=Mg, Fe) coatings for metallic thermal protection systems, Appl. Surf. Sci. 271 (2013) 52–59.
[15] X. He, Y. Li, L. Wang, Y. Sun, S. Zhang, High emissivity coatings for high temperature application: Progress and prospect, Thin Solid Films 517 (2009) 5120–5129.
[16] J.F. Huang, Y.L. Zhang, K.J. Zhu, L.Y. Cao, C.Y. Li, L. Zhou, H.B. Ouyang, B.Y. Zhang, W. Hao, Influence of iodine concentration on microstructure and oxidation resistance of SiB_6–$MoSi_2$ coating deposited by pulse arc discharge deposition, J. Alloy. Compd. 633 (2015) 317–322.
[17] Q. Fu, Y. Shan, C. Cao, H. Li, K. Li, Oxidation and erosion resistant property of SiC/Si–Mo–Cr/$MoSi_2$ multi-layer coated C/C composites, Ceram. Int. 41 (2015) 4101–4107.
[18] G. Shao, X. Wu, Y. Kong, S. Cui, X. Shen, C. Jiao, J. Jiao, Thermal shock behavior and infrared radiation property of integrative insulations consisting of $MoSi_2$/borosilicate glass coating and fibrous ZrO2 ceramic substrate, Surf. Coat. Technol. 270 (2015) 154–163.
[19] M. Wang, X. Li, D. Su, H. Ji, H. Tang, Z. Zhao, J. He, Effect of glass phase content on structure and properties of gradient $MoSi_2$–BaO–Al_2O_3–SiO_2 coating for porous fibrous insulations, J. Alloy. Compd. 657 (2016) 684–690.
[20] A. Vasudevan, J. Petrovic, A comparative overview of molybdenum disilicide composites, Mater. Sci. Eng. A: Struct. 155 (1992) 1–17.
[21] F. Smeacetto, M. Salvo, M. Ferraris, V. Casalegno, G. Canavese, T. Moskalewicz, S. Ellacott, R.D. Rawlings, A.R. Boccaccini, Erosion protective coatings for low density, highly porous carbon/carbon composites, Carbon 47 (2009) 1511–1519.
[22] C. Isola, P. Appendino, F. Bosco, M. Ferraris, M. Salvo, Protective glass coating for carbon-carbon composites, Carbon 36 (1998) 1213–1218.
[23] J.F. Huang, Y.L. Zhang, K.J. Zhu, C.Y. Li, L.Y. Cao, L. Zhou, H.B. Ouyang, B.Y. Zhang, W. Hao, C.Y. Yao, Microstructure and oxidation protection of borosilicate glass coating prepared by pulse arc discharge deposition for C/C composites, Ceram. Int. 41 (2015) 4662–4667.
[24] X. Fei, Y. Niu, H. Ji, L. Huang, X. Zheng, Oxidation behavior of ZrO_2 reinforced $MoSi_2$ composite coatings fabricated by vacuum plasma spraying technology, J. Therm. Spray Technol. 19 (2010) 1074–1080.
[25] W.R. McMahon W.R. McMahon, D.R. Wilder D.R. Wilder, Hemispherical spectral emittance of selected rare earth oxides, J. Am. Ceram. Soc. 51 (1968) 186–192.
[26] Y. Li, W. Zhou, P. Xiao, H. Luo, Z.-l Wen, W. Luo, The anti-oxidation behavior and infrared emissivity property of SiC/$ZrSiO_4$–SiO_2 coating, J. Mater. Sci. Mater. Electron. 25 (2014) 5433–5440.
[27] Y. Yu, R. Luo, Q. Xiang, Y. Zhang, T. Wang, Anti-oxidation properties of a BN/SiC/Si_3N_4–ZrO_2–SiO_2 multilayer coating for carbon/carbon composites, Surf. Coat. Technol. 277 (2015) 7–14.
[28] J. Matsushita, S. Komarneni, High temperature oxidation of silicon hexaboride ceramics, Mater. Res. Bull. 36 (2001) 1083–1089.
[29] G. Shao, X. Wu, Y. Kong, X. Shen, S. Cui, X. Guan, C. Jiao, J. Jiao, Microstructure, radiative property and thermal shock behavior of $TaSi_2$–SiO_2–borosilicate glass coating for fibrous ZrO_2 ceramic insulation, J. Alloy. Compd. 663 (2016) 360–370.
[30] Y.L. Zhang, J.F. Huang, K.J. Zhu, L.Y. Cao, C.Y. Li, L. Zhou, B.Y. Zhang, W.-H. Kong, B. Zhang, Effects of voltage on microstructure and oxidation resistance of SiB_6–$MoSi_2$ coating deposited by pulse arc discharge deposition, Appl. Surf. Sci. 340 (2015) 43–48.
[31] C.W. Bale, E. Belisle, P. Chartrand, S.A. Decterov, G. Eriksson, K. Hack, I.H. Jung, Y.B. Kang, J. Melancon, A.D. Pelton, C. Robelin, S. Petersen, FactSage thermochemical software and databases-recent developments, Calphad 33 (2009) 295–311.

[32] C.-H. Chao, H.-Y. Lu, Stress-induced β→α-cristobalite phase transformation in ($Na_2O+Al_2O_3$)-codoped silica, Mat. Sci. Eng. A: Struct. 328 (2002) 267–276.
[33] G. Kim, I. Sohn, Role of B_2O_3 on the viscosity and structure in the CaO–Al_2O_3–Na_2O-based system, Metall. Mater. Trans. B 45 (2014) 86–95.
[34] D.B. Mahadik, S. Gujjar, G.M. Gouda, H.C. Barshilia, Double layer SiO_2/Al_2O_3 high emissivity coatings on stainless steel substrates using simple spray deposition system, Appl. Surf. Sci. 299 (2014) 6–11.
[35] E. Brodu, M. Balat-Pichelin, J.L. Sans, M.D. Freeman, J.C. Kasper, Efficiency and behavior of textured high emissivity metallic coatings at high temperature, Mater. Des. 83 (2015) 85–94.
[36] S. Le Roux, F. Deschaux-Beaume, T. Cutard, P. Lours, Quantitative assessment of the interfacial roughness in multi-layered materials using image analysis: application to oxidation in ceramic-based materials, J. Eur. Ceram. Soc. 35 (2015) 1063–1079.
[37] C.-D. Wen, I. Mudawar, Modeling the effects of surface roughness on the emissivity of aluminum alloys, Int. J. Heat Mass Transf. 49 (2006) 4279–4289.
[38] W. Peng, Z. Shanbao, Z. Xinghong, G. Kaixuan, L. Yongxia, A. Jiadong, H. Wenbo, Thermal cycling and oxidation resistance of B modified ZrB_2–SiC coatings on SiC coated graphite, Surf. Coat. Technol. 280 (2015) 330–337.
[39] X. Ren, H. Li, Y. Chu, K. Li, Q. Fu, ZrB_2–SiC gradient oxidation protective coating for carbon/carbon composites, Ceram. Int. 40 (2014) 7171–7176.
[40] K.N. Lee, J.I. Eldridge, R.C. Robinson, Residual stresses and their effects on the durability of environmental barrier coatings for SiC ceramics, J. Am. Ceram. Soc. 88 (2005) 3483–3488.
[41] B. Zou, Y. Hui, W. Huang, S. Zhao, X. Chen, R. Xu, S. Tao, Y. Wang, X. Cai, X. Cao, Oxidation protection of carbon/carbon composites with a plasma-sprayed ZrB_2–SiC–Si/Yb_2SiO_5/$LaMgAl_{11}O_{19}$ coating during thermal cycling, J. Eur. Ceram. Soc. 35 (2015) 2017–2025.